Instabilities in a Stratified Fluid Having One Critical Level. Part III: Kelvin–Helmholtz Instabilities as Overreflected Waves

RICHARD S. LINDZEN

Center for Earth and Planetary Physics, Harvard University, Cambridge, MA 02138

ARTHUR J. ROSENTHAL

Department of Mathematics, Massachusetts Institute of Technology, Cambridge, MA 02139

(Manuscript received 17 August 1981, in final form 21 October 1982)

ABSTRACT

We show that Kelvin–Helmholtz instabilities result from overreflected, vertically propagating, vorticity waves. Such waves exist in regions of large vorticity gradients. Just as with gravity wave instabilities, growth rates may be inferred from the quantization and overreflection of such waves. Moreover, overreflection concepts offer convenient insights into why Kelvin–Helmholtz instabilities, when they exist, tend to grow faster than gravity wave instabilities.

1. Introduction

We will show that Kelvin–Helmholtz instabilities may be thought of as overreflected vorticity waves, vertically propagating in regions where the mean flow, $u(z)$, has a large enough curvature that $u_{zz}/(u-c)$ (where c is the phase speed) dominates other terms. The quantization in such regions of the Kelvin–Helmholtz mode enables its value of c_r to be predicted. Also, its overreflection at the height closest to the critical level where it propagates vertically, together with its travel time through the propagation region, enable its growth rate to be estimated. The longer travel time for gravity wave instabilities in stratified shear flow to propagate all the way down to the ground than for Kelvin–Helmholtz instabilities to go down only as far as an internal turning point near the bottom of the shear layer explains why Kelvin–Helmholtz instabilities generally have larger growth rates than coexisting gravity wave instabilities. The larger growth rates are mainly due to the shorter interval between successive overreflections for Kelvin–Helmholtz instabilities than for gravity wave instabilities. (The larger regions of vertical propagation for gravity wave instabilities, on the other hand, help explain the conspicuousness of gravity waves in observations of clear air turbulence.) The overreflection approach has the virtue of clearly identifying instabilities of plane parallel flows as resulting from the interaction of propagating waves with the mean flow. Such interactions are irrelevant to local instabilities like buoyant convection. The contrast between the two types of instability is not evident from normal mode analyses.

2. Model and method

We consider a stably stratified Boussinesq fluid with a plane parallel basic velocity profile $u(z)$ and investigate the behavior of small two dimensional (x and z directions) perturbations, assumed proportional to $\mathrm{Re}\{\exp[ik(x-ct)]\}$, on this basic state. Then, the governing equation for vertical velocity perturbations, $w = \mathrm{Re}\{w(z)\exp[ik(x-ct)]\}$, is

$$\frac{d^2w}{dz^2} + m^2(z)w = 0, \tag{1}$$

where

$$m^2(z) = \frac{N^2(z)}{(u-c)^2} - \frac{u_{zz}}{(u-c)} - k^2 \tag{2}$$

is the square of the local vertical wavenumber $m(z)$; $N^2 = -(g/\rho_0)d\rho_0/dz$ defines the Brunt-Väisälä frequency N (assumed constant unless specifically stated otherwise), g is the gravitational acceleration, $\rho_0(z)$ the basic density distribution, and k the horizontal wavenumber. Also, $c = c_r + ic_i$, where c_r is the phase speed and kc_i the growth rate. For now, we consider the behavior of the solutions to (1) in the limit that $c_i \to 0^+$. Then, it is well established (Lindzen and Rosenthal, 1976, or Part II) that in regions where u is constant and $m^2(z) > 0$, we may have vertically propagating gravity waves, which, for certain horizontal wavenumbers k and phase speeds c_r, may be overreflected, with reflection coefficient R due to a shear layer, down to a lower boundary, which reflects them back to the overreflecting shear layer. With a time interval of 2τ between successive overreflections

at the shear layer, a growth rate kc_i for the instabilities could be predicted using the formula $R = \exp(2kc_i\tau)$.

What we want to show now is that in regions with large vorticity gradient, or large d^2u/dz^2, we have vertically propagating waves which grow as a result of their undergoing multiple overreflections between turning points at the top and bottom of the region having large enough u_{zz} to make $m^2(z) > 0$. To show this quantitatively in the simplest manner possible, we consider a velocity profile in which the region with large u_{zz} is such that $m^2(z)$ is a large positive constant, henceforth called μ_m^2, in this region (assumed to be between $z = 0$ and $z = d$). Below $z = 0$, we let the basic velocity profile have $u(z) = -U$ = constant. At the top of this region, we make the velocity profile have

$$\left.\frac{du}{dz}\right|_{z=d} = \frac{N}{(\mathrm{Ri})^{1/2}}, \tag{3}$$

where $\mathrm{Ri} = N^2/(du/dz)^2$ is the Richardson number at $z = d$. Then, requiring continuity of $u(z)$ and du/dz at $z = 0$ and using the condition

$$\mu^2 \equiv -\frac{u_{zz}}{(u - c_r)} = \text{constant}, \tag{4}$$

which yields nearly constant $m^2(z)$ in $(0, d)$ for large μ^2, results in the basic velocity profile in region $[0, d]$ being

$$u = -(U + c_r)\cos(\mu z) + c_r. \tag{5}$$

Requiring continuity of du/dz at $z = d$ results in μ and d being related by

$$d = \frac{1}{\mu}\arcsin\left[\frac{N}{\mu(\mathrm{Ri}^{1/2})(U + c_r)}\right]. \tag{6}$$

Later, we will find that the way this corner region is rounded has a relatively small effect on the phase speeds and growth rates of the resulting instabilities.

The reason we construct this region $(0, d)$ with constant vertical wavenumber, m, is to ensure well-defined wave propagation, since, as shown by Lindzen *et al.* (1980), when $m(z)$ varies too rapidly, trapping instead of wave propagation can result, even if $m^2(z) > 0$. Also, the constant $m(z)$ enables the group velocity v_g and the travel time τ for the Kelvin–Helmholtz wave to go from $z = 0$ to $z = d$, to be calculated in a straightforward manner. The behavior of the solution around the critical level is determined by assuming a small amount of dissipation to be present. Since the effect of a nonzero c_i is mathematically equivalent to dissipation, we generally integrate the vertical structure equation (1) with a small positive c_i, which henceforth will be referred to as "dissipation." As shown by considering the group velocity of unstable waves (Rosenthal, 1981),

$$v_g = \frac{kc_i}{\mathrm{Im}(m)}, \tag{7}$$

and in the limit as $c_i \to 0$, Eq. (7) gives the usual expression

$$\frac{1}{v_g} = \frac{\partial m}{\partial \omega} = \frac{N^2}{km(u - c_r)^3} - \frac{u_{zz}}{2km(u - c_r)^2}, \tag{8}$$

where $\omega = kc_r$. From (4), (5), (6) and (8) we get

$$\tau = \int_{z=0}^{z=d}\frac{dz}{|v_g|} = \int_{z=0}^{z=d}\left\{\frac{N^2}{km(U + c_r)^3\cos^3\mu z} + \frac{\mu^2}{2km(U + c_r)\cos\mu z}\right\}dz$$

$$= \frac{d}{2km(U + c_r)}\left\{\mu^2 + \left(2 + \frac{1}{6\,\mathrm{Ri}}\right)\frac{N^2}{(U + c_r)^2} + \mathrm{O}\left[\frac{N^4}{\mathrm{Ri}^2\mu^2(U + c_r)^4}\right]\right\}$$

$$\approx \frac{\mu d}{2k(U + c_r)}, \tag{9}$$

where we assume that μ^2 has been picked large enough that $\mu^2 \gg N^2/[\mathrm{Ri}(U + c_r)^2]$, and $c_i^2 \ll (U + c_r)^2$. Since using (7) to get

$$\tau = \frac{d\,\mathrm{Im}(\mu_m)}{kc_i} \tag{10}$$

is less sensitive to the above approximations, we generally use (10) instead of (9) to calculate τ.

In order to have a basic velocity profile approximating the broken line profile of Part I with two regions of high curvature in which a numerical integration can adequately sample the upper region where Kelvin–Helmholtz instabilities are wavelike, we consider a basic velocity profile above $z = d$ with

$$\frac{du}{dz} = \frac{s}{2}\left[1 - \tanh\left(\frac{z - z_B}{L}\right)\right], \tag{11}$$

where $z_B = [\mathrm{Ri}^{1/2}[U - u(d)]/N] + d$ is the height where the upper waveguide region is centered, L gives the thickness of the upper waveguide region, and $s = N/\mathrm{Ri}^{1/2}$ is the slope of $u(z)$ at $z = d$ [as required by (3)], assuming that we pick $L \ll z_B - d$. From (11) and the requirement that $u(z)$ be continuous at $z = d$, we get

$$u(z) = u(d) + 0.5s\left\{z - d - L\log\left[\frac{\cosh[(z - z_B)L^{-1}]}{\cosh[(z_B - d)L^{-1}]}\right]\right\} \tag{12}$$

above $z = d$, where, by (5) and (6),

$$u(d) = -(U + c_r)\cos(\mu d) + c_r \approx -U + \tfrac{1}{2}N\,\mathrm{Ri}^{-1/2}d.$$

From (12) and our choice of L ($L \ll z_B - d$), we note that $\lim_{z\to\infty} u(z) = U$.

Now, it is convenient to define nondimensional

variables obtained by using U as a velocity scale (where U is half the velocity difference between $u(z)$ for $z < 0$ and $u(z)$ for large positive z), N^{-1} as a time scale, and U/N as a length scale, as was done by Lindzen and Rosenthal (1976). For example,

$$\hat{z} = zU/N, \quad \hat{c} = c/U, \quad \hat{k} = kU/N,$$

$$\hat{\tau} = \tau N, \quad \hat{k}\hat{c} = kc/N.$$

Then, all previous equations in this section are valid with these nondimensional variables replacing the corresponding dimensional variables and U and N replaced by the value 1. From now on, we omit the circumflex over nondimensional variables, understanding that all quantities have been nondimensionalized.

Fig. 1 illustrates the basic velocity profile for the sample case Ri = 0.24, L = 0.05, μ^2 = 250, and k = 1.2, when the value of c_r used to compute d with (6) and evaluate (12) is that possessed by the Kelvin–Helmholtz instability for these parameters. (Now, it turns out that c_r = 0.001705 and c_i = 0.009581; from (6), d = 0.0081738). We will later explain in detail the algorithm used to find c_r and c_i. For now, we note that the velocity profile as shown in Fig. 1 varies only slightly as c_r is varied.

The near constancy of $m^2(z)$ at the value $\mu_m{}^2$ in the interval [0, d] (as illustrated by Fig. 2), enables us to consider Kelvin–Helmholtz instabilities as vertically propagating vorticity waves with constant vertical wavenumber there. We now show how reflection

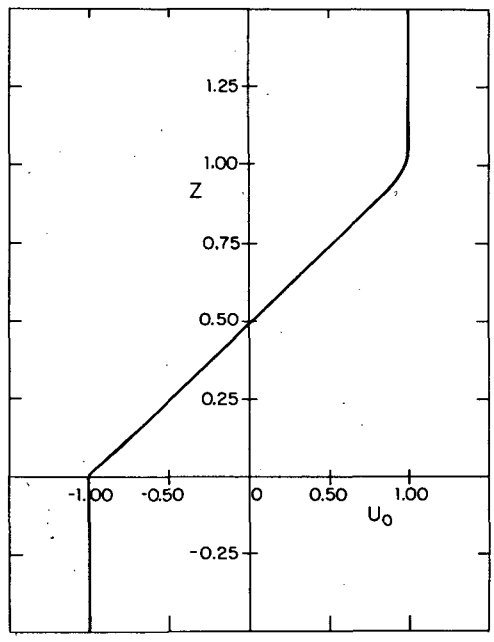

FIG. 1. Basic state velocity profile $u_0(z)$ when Ri = 0.24, μ^2 = 250, d = 0.0081738, k = 1.2, L = 0.05. [Then, it turns out that $(c_r)_{cig}$ = 0.00170494 and $(c_i)_{cig}$ = 0.009581.]

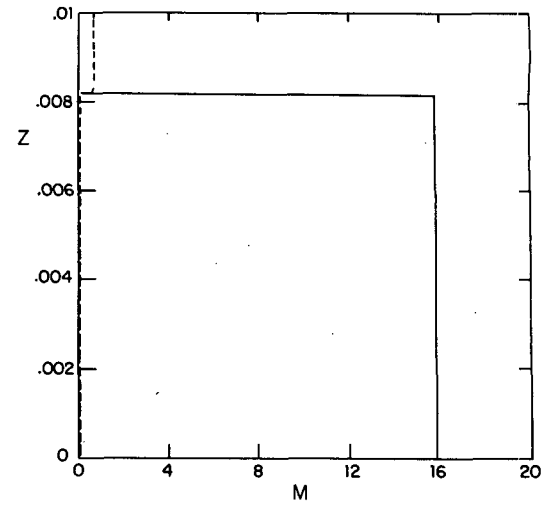

FIG. 2. Vertical wavenumber m versus height z in the region where $(-u_0)_{zz}/(u_0 - c_r) = \mu^2$ = 250 = constant, for the velocity profile in Fig. 1. The solid line shows |Rem| and the dashed curve shows |Imm| (i.e., the decay scale in height).

coefficients and quantization conditions can be calculated for these vorticity waves and then used to explain the growth rates of the resulting Kelvin–Helmholtz instabilities. We write the solution to (1) in the region [0, d] as

$$w = \exp(-i\mu_m z) + R\exp(i\mu_m z), \tag{13}$$

where, with the branch of μ_m chosen such that $\mathrm{Re}(\mu_m) > 0$ (and $\mathrm{Im}(\mu_m) \leq 0$), the term $\exp(-i\mu_m z)$ represents an incident wave with upgoing energy propagation and the term $R\exp(i\mu_m z)$ represents a reflected wave with downgoing energy propagation. We now want to find the reflection coefficient $|R|$ which will enable us to predict growth rates. To do this, we need to know how the solution interacts with the critical level, where the phase speed of the wave, c_r, equals the speed of the mean flow, $u(z)$. The way this interaction is calculated now involves integrating (1) with a small amount of damping [i.e. a small positive c_i, henceforth called $(c_i)_{\mathrm{orig}}$] introduced to enable the integration to pass through the critical level, where without the positive c_i, (1) would have a singularity.

This integration is done using Gaussian elimination, as described by Lindzen and Kuo (1969) or Lindzen *et al.* (1980). We choose a height z_T (typically z_T = 2) at which the integration starts and define M + 1 grid points by $z_n = z_T - nh$ ($0 \leq n \leq M$), where $h = (z_T - d)/M$. In order that the smoothed singularity at the critical level be resolved, we require that

$$h < \frac{(c_i)_{\mathrm{orig}}}{|du/dz|_{z=z_c}} = (c_i)_{\mathrm{orig}}(\mathrm{Ri}^{1/2}), \tag{14}$$

where Ri is the Richardson number at the critical level z_c. ($\mathrm{Ri}(z_c) \approx \mathrm{Ri}(d)$). Also, in order that the prop-

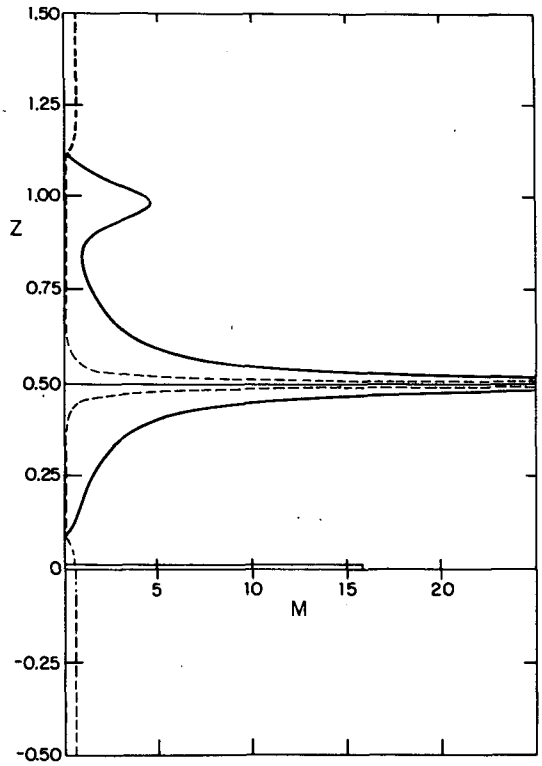

FIG. 3. Vertical wavenumber m versus height. The notation used is the same as in Fig. 2.

erties of the waveguide region near $z = z_B$, where Kelvin–Helmholtz waves can propagate vertically due to the large vorticity gradient, be resolved, we require $2h < L$. For a typical case with Ri = 0.24, $L = 0.05$ and $(c_i)_{\text{orig}} = 0.004$, we find that $M = 3000$ points are sufficient to satisfy these criteria.

After using centered differences to approximate d^2w/dz^2 in (1), we get the following finite difference approximation for (1)

$$w_{n+1} + (Q_n h^2 - 2)w_n + w_{n-1} = 0, \quad n = 1, 2, \ldots, M-1. \tag{15}$$

Here, the subscript n refers to evaluation at $z = z_n$ and $Q(z) = m^2(z)$. To solve (15), we let

$$w_{n-1} = \alpha_n w_n, \quad n = 1, 2, \ldots, M, \tag{16}$$

and get

$$w_{n+1}[1 + (Q_n h^2 - 2)\alpha_{n+1} + \alpha_n \alpha_{n+1}] = 0$$

from (15). As long as no interior point is a zero of w, this yields

$$\alpha_{n+1} = \frac{1}{2 - \alpha_n - Q_n h^2}, \quad n = 1, 2, \ldots, M-1. \tag{17}$$

To obtain the value of α_1 needed to start using the recursion formula (17), we invoke our upper boundary condition. We consider two possibilities:

1) There is a rigid lid at $z = z_T$. Then $w_0 = 0$, and we get from (15) and (16) that $\alpha_1 = 0$.

2) There is no upper boundary and z_T is high enough to be in the region where $(-m^2(z))$ has a nearly constant value, henceforth called n_T^2.

As shown in Fig. 3, any value of z_T greater than 1.3 will satisfy this criterion in our sample case. Now, we require the solution for large z to be of the form

$$w = A_T \exp(-n_T z), \tag{18}$$

where A_T is a constant, and we pick the square root of n_T^2 having $\text{Re}(n_T) \geq 0$ and $(\text{Im}n_T)(1 - c_r) \leq 0$. This solution is consistent with the condition of exponential decay as $z \to \infty$, which is appropriate when $(c_i)_{\text{orig}} > 0$ or when considering Kelvin–Helmholtz instabilities. It is also consistent with the radiation condition for gravity waves propagating upwards to large positive z when this is appropriate. From (18), we get $dw/dz = -n_T w$, or in centered finite difference form at $z = z_T$,

$$(w_{-1} - w_1)/2h = -n_T w_0, \tag{19}$$

where the definition $w_n = w(z_T - nh)$ has been extended to define $w_{-1} = w(z_T + h)$. From (15) applied at $z = z_T$, we have

$$w_1 - (n_T^2 h^2 + 2)w_0 + w_{-1} = 0. \tag{20}$$

Eliminating w_{-1} from (19) and (20), and then using (16) yields

$$\alpha_1 = \frac{2}{(2 + 2n_T h + n_T^2 h^2)}. \tag{21}$$

After obtaining α_1, and sweeping down with the recursion formula (17) to get $\alpha_2, \ldots, \alpha_M$, we next invoke the conditions of continuity of displacement {i.e., of $w/(u - c)$} and pressure {i.e., of $[(u - c)dw/dz - wdu/dz]\rho_0/ik$} at $z_M = d$ to get, using (13),

$$w_M = \exp(-i\mu_m d) + R \exp(i\mu_m d), \tag{22}$$

$$\left.\frac{dw}{dz}\right|_{z=d^+} \approx \frac{w_{M-1} - w_M}{h} = -i\mu_m \exp(-i\mu_m d) + i\mu_m R \exp(i\mu_m d) = \left.\frac{dw}{dz}\right|_{z=d^-}. \tag{23}$$

Since $w_{M-1} = \alpha_M w_M$, we can eliminate w_M from (22) and (23) and solve for R to get

$$R = \frac{(1 - \alpha_M - i\mu_m h)}{(\alpha_M - 1 - i\mu_m h)} \exp(-2i\mu_m d). \tag{24}$$

(Then, if desired, we could use (22) and $w_{n-1} = \alpha_n w_n$ for $n = M, M-1, \ldots, 2$ to sweep up from $z = d$ to $z = z_T$ and get the solution for w at all grid points in this range.)

From (13) and (24), we find that the ratio of the amplitude of the downward propagating, reflected wave to that of the upward propagating, incident wave just below $z = d$ is the norm of a reflection coefficient, henceforth called R_{sweep}, given by

$$R_{\text{sweep}} = \frac{R\exp(i\mu_m d)}{\exp(-i\mu_m d)} = \frac{(1-\alpha_M - i\mu_m h)}{(\alpha_M - 1 - i\mu_m h)}. \quad (25)$$

To obtain an appropriate value of c_r at which to evaluate R_{sweep}, we invoke a quantization condition involving matching the phase of the incident wave, $\exp(-i\mu_m z)$, and of the reflected wave, $R\cdot\exp(i\mu_m z)$, at the top of the region $[0, d]$. [This quantization is analogous to the quantization for gravity wave instabilities noted by Lindzen and Rosenthal (1976), which turned out to restrict the number of vertical half-wavelengths between the bottom of the shear zone and the ground to values separated by integers.] Quantitatively, obtaining the quantization condition involves invoking a lower boundary condition at $z = 0$, which now is more complicated than just saying there is a rigid boundary at $z = 0$. The solution just above $z = 0$ given by (13) must match the displacement and pressure perturbations of a solution below $z = 0$ having the form

$$w = A_r\exp(n_B z) + A_i\exp(-n_B z), \quad (26)$$

where $(-n_B^2)$ is the constant value $m^2(z)$ [given by (2)] has below $z = 0$, and we pick the square root of n_B^2 having $\text{Re}(n_B) \geq 0$ and $(\text{Im}n_B)(1 + c_r) \geq 0$. Then, if no lower boundary is present, we must have $A_i = 0$, to be consistent with boundedness of w as $z \to -\infty$ and the radiation condition that only downward propagating waves be present when $n_B^2 < 0$ and there is no lower boundary. Continuity of displacement of the solutions represented by (13) and (26) at $z = 0$ implies

$$w(0^+) = 1 + R = A_r + A_i = w(0^-). \quad (27)$$

Continuity of pressure at $z = 0$ implies

$$\left.\frac{dw}{dz}\right|_{z=0^+} = i\mu_m(R-1) = n_B(A_r - A_i) = \left.\frac{dw}{dz}\right|_{z=0^-}. \quad (28)$$

To eliminate A_r and A_i from (27) and (28), we need to invoke our lower boundary condition. We consider two possibilities:

1) There is no ground present. Then, $A_i = 0$ and (27) and (28) give

$$R = -\frac{(n_B + i\mu_m)}{(n_B - i\mu_m)} = -\frac{(n_B^2 - \mu_m^2 + 2in_B\mu_m)}{(n_B^2 + \mu_m^2)}. \quad (29)$$

This yields, using (22), that the ratio of the amplitude of the downward propagating, reflected wave to that of the upward propagating incident wave just below $z = d$ is the norm of a reflection coefficient, henceforth called R_{match}, given by

$$R_{\text{match}} = \frac{R\exp(i\mu_m d)}{\exp(-i\mu_m d)} = -\frac{(n_B^2 - \mu_m^2 + 2in_B\mu_m)}{(n_B^2 + \mu_m^2)}\exp(2i\mu_m d). \quad (30)$$

When c_r is such that the phase of R_{match} in (30), henceforth called θ_m, equals the phase of R_{sweep} in (25), henceforth called θ_{sweep}, quantization is satisfied.

2) The second possibility is that a lower boundary is present at a nondimensional distance H below the bottom of the shear layer. (Then, the nondimensional distance of the ground below the center of the shear layer is $H + \text{Ri}^{1/2}$). Now, our lower boundary condition is

$$w(z = -H) = 0, \quad (31)$$

which yields, using (26), that

$$A_i = -A_r\exp[-2n_B H]. \quad (32)$$

From (27) and (28) we get

$$R = -\frac{\{n_B[1 + \exp(-2n_B H)] + i\mu_m[1 - \exp(-2n_B H)]\}}{\{n_B[1 + \exp(-2n_B H)] - i\mu_m[1 - \exp(-2n_B H)]\}} = -\frac{\{n_B\cosh(n_B H) + i\mu_m\sinh(n_B H)\}}{\{n_B\cosh(n_B H) - i\mu_m\sinh(n_B H)\}}. \quad (33)$$

Hence, the ratio of the amplitude of the downward propagating, reflected wave to that of the upward propagating, incident wave just below $z = d$ is the norm of a reflection coefficient, R_{match}, now given by

$$R_{\text{match}} = \frac{[R\exp(i\mu_m d)]}{[\exp(-i\mu_m d)]} = -\frac{[n_B\cosh(n_B H) + i\mu_m\sinh(n_B H)]}{[n_B\cosh(n_B H) - i\mu_m\sinh(n_B H)]} \times \exp(2i\mu_m d). \quad (34)$$

To interpret physically the quantization condition that θ_m, the phase of R_{match} in (34) equals θ_{sweep}, the phase of R_{sweep} in (25), we consider what happens as $|R| \to 1$. Then, $R \approx \exp(i\theta)$, and from matching the solutions represented by (26) and (13) at $z = 0$, and defining $m_B = -in_B$, we obtain

$$\theta_{\text{sweep}} = \theta_m \approx 2\mu_m d - 2\tan^{-1}\left\{\frac{n_B}{\mu_m\tanh(n_B H)}\right\} + 2I_1\pi = 2\mu_m d - 2\tan^{-1}\left\{\frac{m_B}{\mu_m\tan(m_B H)}\right\} + 2I_1\pi, \quad (35)$$

where I_1 is an integer. From (35), we see that, if when $m_B H = \phi$, where ϕ is some number, quantization is satisfied, then the family of modes of gravity waves with $m_B H \approx \phi + I\pi$, where I is an integer, will also satisfy quantization (if we vary μ_m to keep m_B/μ_m constant as m_B varies). As shown later, when $\mu_m \gg 1$, the values of c_r and c_i for instabilities are relatively insensitive to μ_m. This means the number of half wavelengths between the bottom of the shear zone and the ground is of the form $I + \phi/\pi$, where ϕ is the value of $m_B H$ for one of the modes.

Although (35) helps give a physical interpretation of the quantization condition, it can be shown (Rosenthal, 1981) that any nonzero $(c_i)_{\text{orig}}$, no matter how small, adversely affects the accuracy of (35). Hence, we compute the phase of R_{match} using (34) rather than (35) to avoid significant inaccuracy in c_r found from our quantization condition $\theta_{\text{sweep}} = \theta_m$. This phenomenon of a small $(c_i)_{\text{orig}}$ affecting results also occurs when no lower boundary is present and when the solution is evanescent below the shear layer.

After a phase speed c_r has been found that satisfies our quantization condition ($\theta_m = \theta_{\text{sweep}}$) and R_{sweep} (the reflection coefficient just below $z = d$) has been computed using (25), the growth rate can be predicted from overreflection after calculating r_{bot}, the reflection coefficient just above $z = 0$, the bottom of the region of high curvature. (Due to $(c_i)_{\text{orig}}$ being nonzero, r_{bot} turns out to be significantly less than 1, even for Kelvin–Helmholtz modes which would not propagate at all below the shear layer with c_i zero.) From (22), we find that r_{bot}, the ratio of the amplitude of the upward propagating, reflected wave, to that of the downward propagating, incident wave, just above $z = 0$ is

$$r_{\text{bot}} = \frac{1}{|R|}, \tag{36}$$

where R is given by (29) when there is no ground present, or by (33) when there is a lower boundary present. We now have

$$r_{\text{bot}}\mathrm{R}_{\text{sweep}} = \exp[2k(c_i)_{\text{pred},rR}\tau_{\text{orig}}], \tag{37}$$

where

$$k(c_i)_{\text{pred},rR} = \frac{[\ln(r_{\text{bot}}\mathrm{R}_{\text{sweep}})]}{2\tau_{\text{orig}}} \tag{38}$$

estimates the growth rate from overreflection using both r_{bot} and $\mathrm{R}_{\text{sweep}} \equiv |R_{\text{sweep}}|$.

For gravity wave instabilities in the case with a lower boundary present, we can also predict the growth rate from

$$\mathrm{R}_g = \exp[2k(c_i)_{\text{pred},g}\tau_g], \tag{39}$$

where τ_g is the travel time for a wave to go from $z = 0$ down to the ground at $z = -H$ and R_g is the ratio of the amplitude of the downward propagating, reflected wave to that of the upward propagating, incident wave just below $z = 0$. We have

$$\tau_g = \int_{z=-H}^{z=0} \frac{dz}{|v_g|},$$

where we could use the value of v_g, the group velocity between the bottom of the shear layer and the ground, from (8), given by

$$v_g = km_B(1 + c_r)^3, \tag{40}$$

which is valid if $(c_i)_{\text{orig}}$ is close to 0 and $|\mathrm{Im}m_B| \ll |\mathrm{Re}m_B|$. Since using (7) to get

$$v_g = \frac{[k(c_i)_{\text{orig}}]}{|\mathrm{Re}n_B|}, \tag{41}$$

and then

$$\tau_g = \frac{[H|\mathrm{Re}n_B|]}{[k(c_i)_{\text{orig}}]} \tag{42}$$

is less sensitive to the above approximations, we generally use (42) instead of (40) to evaluate τ_g.

The reflection coefficient R_g applicable just below the bottom of the shear layer can be readily calculated from the value of R given by (33). From (27) and (28), we have

$$\frac{(A_r + A_i)}{(A_r - A_i)} = R_t, \tag{43}$$

where

$$R_t = \frac{[n_B(1 + R)]}{[i\mu_m(R - 1)]}. \tag{44}$$

Then, using (26), we find that R_g is the norm of R_g, where

$$R_g = \frac{A_r}{A_i} = \frac{R + 1}{R_t - 1} = \frac{n_B(1 + R) + i\mu_m(R - 1)}{n_B(1 + R) - i\mu_m(R - 1)}. \tag{45}$$

Thus, to predict the growth rate of gravity wave instabilities, we use the following formula, based on overreflection after each round trip from the ground to the shear zone as the physical mechanism for amplification [as in (39)]:

$$k(c_i)_{\text{pred},g} = \frac{\ln \mathrm{R}_g}{(2\tau_g)}. \tag{46}$$

It is straightforward to show that the quantization condition that the phase of A_r/A_i from (32) (namely, Phase $[-\exp(2n_B H)] = (2I + 1)\pi + 2(\mathrm{Im}n_B)H$, where I is an integer) be the same as the phase of R_g in (45) is equivalent to the quantization condition that the phase of R_{match} in (34) be the same as the phase of R_{sweep} in (25). The reason we use (45) rather than

$$\frac{A_r}{A_i} = -\exp(2n_B H) \tag{47}$$

from (32) to define R_g is that (47) used with (46) would yield the unhelpful result $(c_i)_{\text{pred},g} = (c_i)_{\text{orig}}$, since (47) incorporates none of the behavior of the basic velocity profile above the bottom of the shear layer or around the critical level. Also, we should not

anticipate that just using (45) with (46) would yield the best possible estimate of the growth rate, because R_g given by (45) does not involve the behavior of the basic velocity profile below the bottom of the shear layer. Later, we shall describe a more accurate method of calculating R_g and predicting the growth rate which incorporates the effect of the entire basic velocity profile.

3. Results and discussion

We first consider the sample case illustrated in Fig. 1 of a fluid with no lower boundary, and with a Richardson number Ri of 0.15 at $z = d$, right above the top of the lower region of high curvature.

Our first estimate of the growth rate from overreflection is

$$k(c_i)_{\text{pred},rR} = \frac{\ln(r_{\text{bot}}R_{\text{sweep}})}{2\tau_{\text{orig}}}$$

as given by (38). Fig. 4 shows the result, which turns out to be general, that the neutral points predicted from the overreflection formula (38) agree well with the neutral points found in Part I using the dispersion relation for the broken line profile. (The broken line profile could be represented by the velocity profile given in the previous section by (12) in the limiting case that $d \to 0$, $L \to 0$, and $\mu^2 \to \infty$.) From (38) we see that overreflection is equivalent to a positive value of $k(c_i)_{\text{pred},rR}$, which in turn, according to Fig. 4, corresponds to positive growth rates from the dispersion relation.

However, Fig. 4 also shows that $k(c_i)_{\text{pred},rR}$ overestimates the growth rate from the dispersion relation, henceforth called the dispersion growth rate, by a factor of more than 3. Thus, the mechanism of overreflection can result in more than enough growth to account for the actual dispersion growth rate.

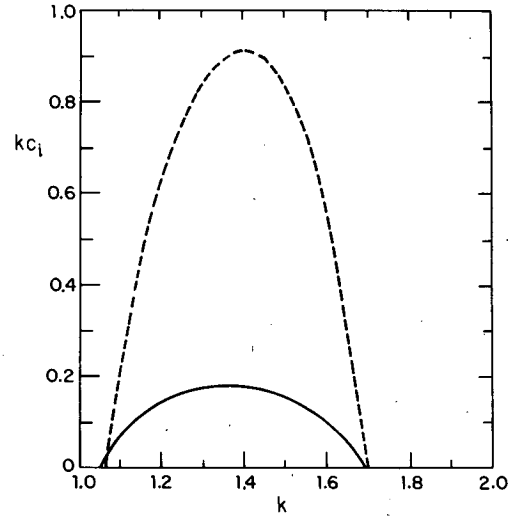

FIG. 4. Growth rate versus wavenumber for the case Ri = 0.15, no ground, $(c_i)_{\text{orig}} = 0.02$, $L = 0.1$, $\mu^2 = 900$. A radiation condition is used at $z_T = 1.4$. The solid line shows $k(c_i)_{\text{disp}}$, found from the dispersion relation for this profile in the limit $L \to 0$, $\mu \to \infty$. The dashed line shows $k(c_i)_{\text{pred},rR}$ [$=\ln(r_{\text{bot}}R_{\text{sweep}})/(2\tau_{\text{orig}})$] from (38).

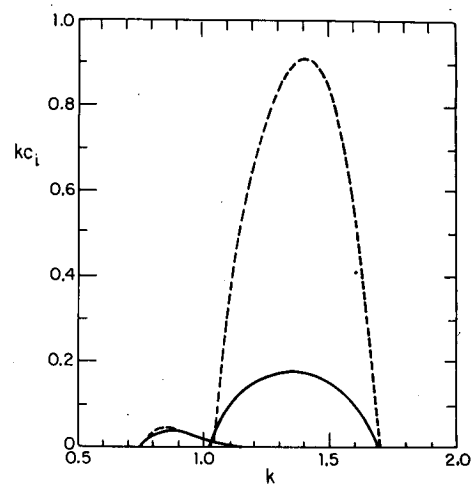

FIG. 5. As in Fig. 4, except $\hat{H} = 3.24$ and the dashed line for the gravity wave mode shows $k(c_i)_{\text{pred},g}$ [$=\ln R_g/(2\tau_g)$ from (46)].

We also obtain similar results when there is a lower boundary at a distance $\hat{H}$ below the center of the shear zone, as shown in Fig. 5 for the sample case $\hat{H} = 3.24$, except that now gravity wave instabilities which propagate below the bottom of the shear zone down to the ground are also found. For clarity, we only show in Fig. 5 the gravity wave mode whose number of vertical half-wavelengths between the bottom of the shear zone and the ground, the mode number, is close to 1, even though gravity waves with mode numbers 2, 3, etc. are also found. For $\hat{H} = 3.24$ (and also all other values of $\hat{H}$ less than 6), the mode number 1 gravity-wave instability has the largest growth rate predicted from overreflection of all gravity-wave modes, but these growth rates are less than those of the most unstable Kelvin–Helmholtz instability at the same Ri.

In Figs. 6 and 7, we show that the values of the phase speed, c_r, found from the quantization condition that the phase of R_{sweep}, given by (25), equal the phase of R_{match}, given by (30) (when no lower boundary is present, as in Fig. 6) or (34) (when a lower boundary is present, as in Fig. 7) agree well with the values of the dispersion phase speed. We also show in these two figures, with a line with embedded +'s, the values of c_r, henceforth called the eigenvalue phase speed, obtained by using a two dimensional secant method (Lindzen and Rosenthal, 1976) to find the values of c_r and c_i that make the complex numbers R_{sweep} and R_{match} equal. The superb agreement of the dispersion phase speed, found for a broken line profile in the limiting case $L \to 0$ and $\mu^2 \to \infty$, with the eigenvalue phase speed, which is actually the phase speed that is applicable to the dis-

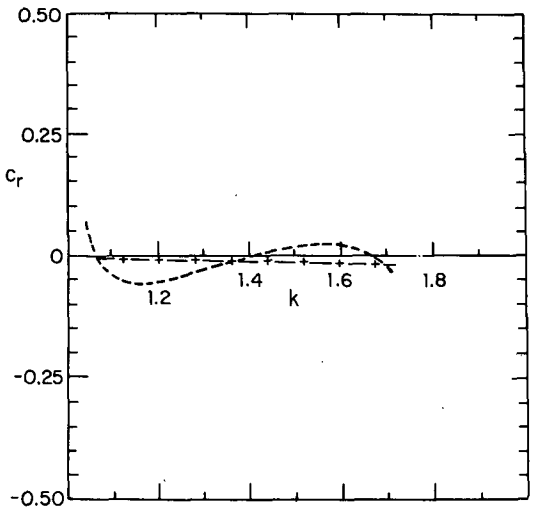

FIG. 6. Phase speed versus wavenumber for the case shown in Fig. 4. The solid line (which nearly coincides with $c_r = 0$ now) shows $(c_r)_{\text{disp}}$. The dashed line shows $(c_r)_{\text{quantization}}$ [i.e., the c_r at which the phase of R_{match} equals the phase of R_{sweep} at $(c_i)_{\text{orig}}$]. The line with embedded +'s shows $(c_r)_{\text{eig}}$ [i.e., the c_r at which $R_{\text{match}} = R_{\text{sweep}}$. This occurs at $(c_i)_{\text{eig}}$].

persion relation for the profile used with $L = 0.1$ and $\mu^2 = 900$, shows the unimportance of the parameters L and μ. *The only reason we choose L nonzero and μ finite is to allow the effects of the vorticity gradient near the corners of the basic u profile to be investigated in detail.*

Although our initial estimate of the growth rate, $k(c_i)_{\text{pred},rR}$, is much larger than the dispersion growth rate, our initial growth rate estimates still can be successful qualitatively in explaining several properties of Kelvin–Helmholtz and gravity wave instabilities. In Fig. 8, we show the behavior of the reflection coefficient R_{sweep} versus c_r at several different wavenumbers for the case Ri = 0.15 and $\hat{H} = 3.24$. To clarify the negligible role of the parameters L and μ in qualitatively determining our growth rate results, we have taken several values of μ in these figures. At $k = 0.78$, which is slightly greater than the smallest unstable wavenumber for mode 1 gravity wave instabilities, the value of c_r for which quantization occurs (henceforth indicated with a "Q") lies slightly inside the range of c_r's for which $R_{\text{sweep}} > 1$. As k increases to 0.8675, the most unstable wavenumber for mode 1 gravity wave instabilities, as in Fig. 8b, the curve of R_{sweep} versus c_r shifts to the right so as to make the c_r at which quantization occurs have a larger R_{sweep}. However, as shown by Fig. 8c for $k = 1$ (which has a dispersion growth rate less than half that at $k = 0.8675$), the wavenumber which is most unstable does not coincide with the wavenumber for which the c_r that satisfies quantization occurs where the reflection coefficient is maximal. As discussed by Lindzen and Rosenthal (1976), this coincidence of the c_r that gives maximal growth from overreflection with the c_r satisfying quantization at the most unstable wavenumber only occurs for gravity wave instabilities at certain ground to shear layer distances $\hat{H}$.

Figs. 8a–8c indicate that for wavenumbers k less than 1, we have $R_{\text{sweep}} < 1$ for phase speeds c_r near 0, which correspond to a critical level near the middle of the shear layer, as would be appropriate for Kelvin–Helmholtz disturbances. Thus, there are no Kelvin–Helmholtz instabilities present when $k < 1$. On the other hand, Figs. 8d–8f indicate that for larger wavenumbers up to 1.69, we do have overreflection ($R_{\text{sweep}} > 1$) for phase speeds c_r near 0 that Kelvin–Helmholtz disturbances have, but we no longer have overreflection for phase speeds c_r near −0.4 that gravity waves have. This is consistent with the lack of instability of gravity waves and the instability of Kelvin–Helmholtz disturbances at these higher wavenumbers. Fig. 8e for the case $k = 1.35$, which is the wavenumber at which Kelvin–Helmholtz disturbances have the largest dispersion growth rate, indicates the following result, which seems to be general: The wavenumber at which the R_{sweep} curve is such that its maximum occurs at the value of c_r for which Kelvin–Helmholtz disturbances are quantized [*viz*, ≈ 0, as long as the ground isn't too close to the bottom of the shear layer (i.e., $\hat{H} > 2$)] is the most unstable wavenumber.

Analysis of graphs such as Fig. 8 shows that the values of R_{sweep} are not generally greater for Kelvin–Helmholtz instabilities than for gravity wave instabilities, despite the greater dispersion growth rates for Kelvin–Helmholtz instabilities than for gravity wave instabilities. To fully explain the greater dispersion growth rates for the Kelvin–Helmholtz instabilities, we must consider the effects of the partial reflection

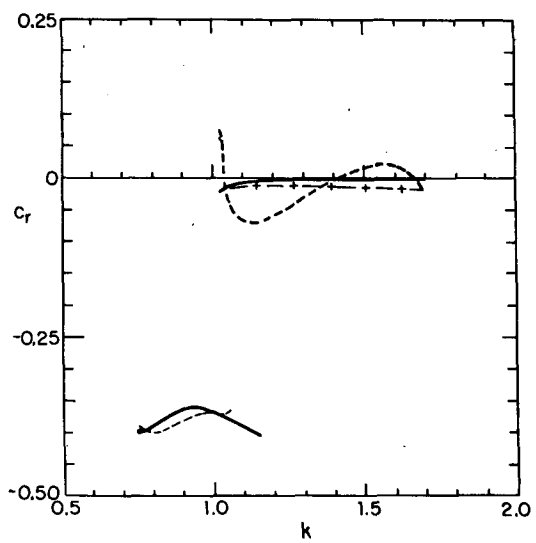

FIG. 7. As in Fig. 6, except $\hat{H} = 3.24$.

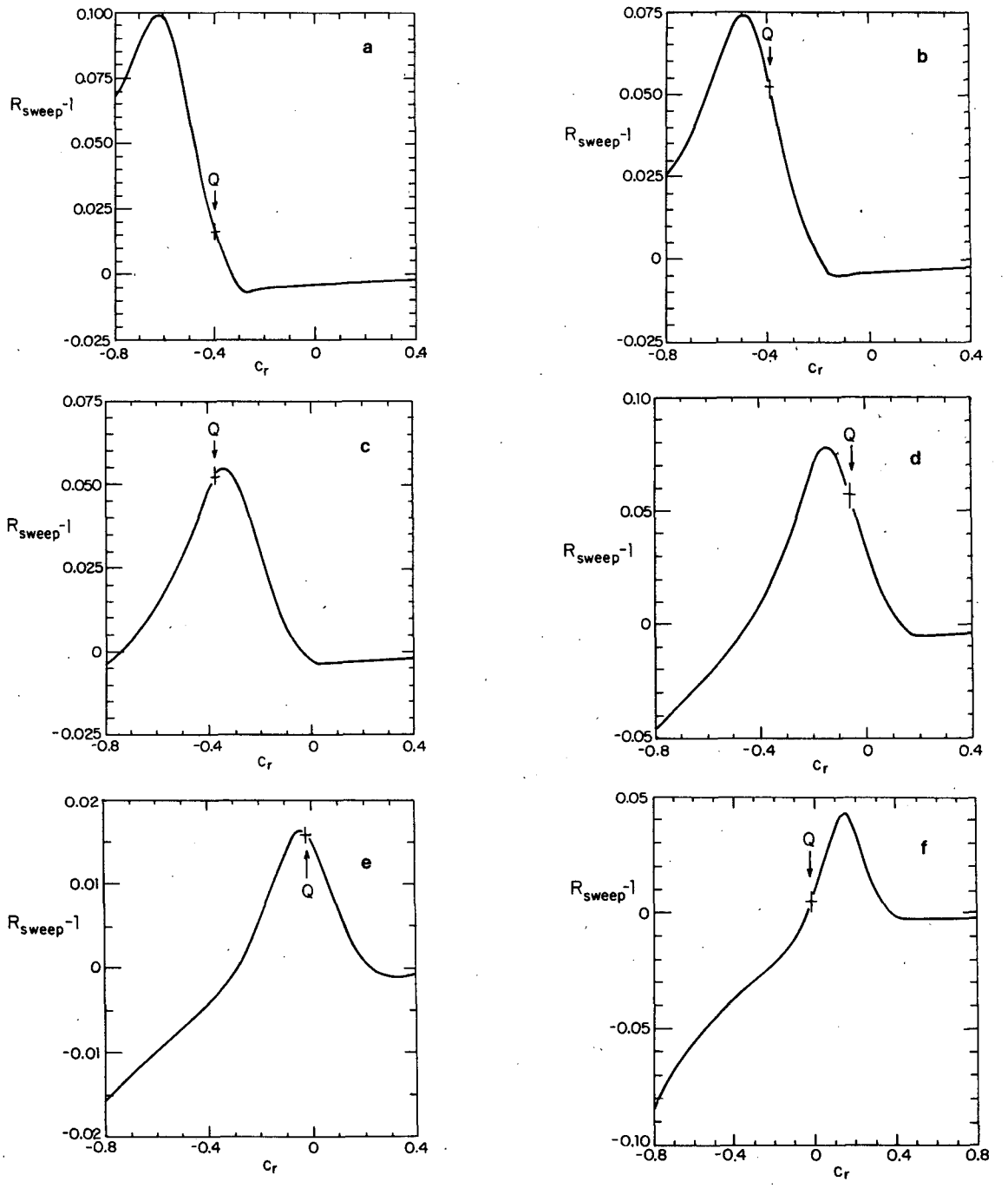

FIG. 8. $R_{sweep} - 1$ versus c_r for the case Ri = 0.15, $(c_i)_{orig}$ = 0.02, L = 0.1. The c_r at which quantization occurs has been labeled with a Q. (a) k = 0.78, μ^2 = 3332; (b) k = 0.8675, μ^2 = 3332; (c) k = 1, μ^2 = 3332; (d) k = 1.2, μ^2 = 900; (e) k = 1.35, μ^2 = 13697; (f) k = 1.69, μ^2 = 900.

at the lower turning point, as given by r_{bot}, and of the travel time τ_{orig} between the turning points. For example, when $\hat{H}$ = 3.24, Ri = 0.15, $(c_i)_{orig}$ = 0.02, μ^2 = 900, and L = 0.1, we see from Table 1 that, even though the reflection coefficient R_{sweep} for the most unstable gravity wave is larger than for the most unstable Kelvin–Helmholtz instability, the predicted gravity wave growth rate from overreflection, $(c_i)_{pred,rR}$, is less than half the predicted Kelvin–Helmholtz growth rate. This can be explained by noting that the

TABLE 1. Properties of the most unstable gravity wave and Kelvin–Helmholtz instabilities when $\hat{H} = 3.24$, Ri $= 0.15$, $(c_i)_{orig} = 0.02$, $\mu^2 = 900$, and $L = 0.1$.

	Gravity wave	Kelvin–Helmholtz
k	0.8675	1.3529
$(c_r)_{quantization}$	−0.389	−0.015
R_{sweep}	1.1035	1.0629
r_{bot}	0.97250	0.99790
Vertical group velocity v_g in $(0, d)$	0.0348	0.0883
Travel time, $z = 0$ to $z = d$: τ_{orig}	0.135	0.0331
d	0.00471	0.00292
$(c_i)_{pred,rR}$	0.3006	0.6588
Reflection coefficient, R_g below $z = 0$	2.55348	
v_g below $z = 0$	0.2742	
Travel time, $z = 0$ to ground: τ_g	10.403	
$(c_i)_{pred,g}$ (from R_g and τ_g)	0.05205	
Dispersion relation:		
$(c_r)_{disp}$	−0.3701	−0.0014
$(c_i)_{disp}$	0.0461	0.1310
Overreflection:		
$(c_i)_2$ [from (A3)]	0.0482	0.1691
$(c_i)_F$	0.0438	0.1317
$(c_r)_{eig}$	−0.37	−0.0126
$(c_i)_{eig}$	0.046	0.1323
$(R_g)_{eff} = \exp[2k(c_i)_{disp}\tau_g]$	2.29242	
$(R_{sweep})_{eff} = \exp[2k(c_i)_{disp}\tau_{orig}]$		1.0118
at $(c_i)_{orig}$ n_B	0.0632 + 1.38i	0.895 + 0.0234i
at $(c_i)_{orig}$ n_T	0.485 − 0.0154i	0.928 − 0.0206i
at $(c_i)_{orig}$ μ_m	30. − 0.498i	30. − 0.307i

vertical group velocity of the gravity wave instability is less than half that of the Kelvin–Helmholtz instability in the region of high vorticity gradient. This in turn implies that gravity waves undergo overreflection less often than Kelvin–Helmholtz instabilities. Also, the gravity wave instability suffers much more leakage from the bottom of the region of high curvature than the Kelvin–Helmholtz instability, as is shown by the values of r_{bot} in Table 1.

Alternatively, we can calculate the growth rate of the gravity wave instability from its reflection coefficient below $z = 0$. From (45), we find $R_g = 2.553$ and from (42), we find $\tau_g = 10.403$, even though, from (41), $v_g = 0.2742$ is larger than the vertical group velocity for the Kelvin–Helmholtz instability in the region of high vorticity gradient. This much larger travel time $2\tau_g = 20.8$ for the gravity wave instability to travel the large distance between the bottom of the shear zone and the ground and back than for the Kelvin–Helmholtz instability to travel its short distance $2d$ between successive overreflections is responsible for the smaller predicted value of $(c_i)_{pred,g} = 0.0521$ for the gravity wave instability than $(c_i)_{pred,rR} = 0.6588$ for the Kelvin–Helmholtz instability.

We can apply the above ideas to explain what happens to Kelvin–Helmholtz instabilities as the distance between the ground and shear layer $\hat{H}$ decreases to values less than 3. As noted in Part I, as $\hat{H}$ decreases, the phase speed c_r for quantization of Kelvin–Helmholtz instabilities decreases. Since the reflection coefficient R_{sweep} is independent of $\hat{H}$, for given k, Ri and $(c_i)_{orig}$, we see from graphs such as Figs. 8c and 8d that as $\hat{H}$ decreases, the value of k at which the maximum value of R_{sweep} occurs above our quantization c_r must decrease. This is because the R_{sweep} versus c_r curves (as in Fig. 8) move to the left (i.e. towards lower c_r) as k decreases. Hence, considering overreflection makes us expect that the most unstable wavenumber for Kelvin–Helmholtz instabilities at a given Ri will decrease as $\hat{H}$ decreases. This behavior was found in Part I. Moreover, the tendency of R_{sweep} to become larger at the smaller wavenumbers (as shown by Figs. 8a–8c) for constant $(c_i)_{orig}$, Ri and μ, accounts for why the maximal growth rate for Kelvin–Helmholtz instabilities could increase for a while as $\hat{H}$ decreases down to 2, as shown by Fig. 12 in Part I. As $\hat{H}$ decreases below 2, the tendency for τ_{orig} to increase at the resulting smaller c_r's (as shown by Fig. 9) becomes the predominant effect, and helps explain why the maximal growth rate of Kelvin–Helmholtz instabilities decreases drastically to 0 then, as shown by Fig. 12 in Part I.

To discover a physical mechanism which could account for our initial estimates of growth rates from overreflection usually being overestimates of the dispersion growth rate, we note that integrating the differential equation (1) with a value of $(c_i)_{orig}$ implies that the resulting calculated reflection coefficients are given a time of order $(k(c_i)_{orig})^{-1} \equiv \tau_0$ to develop. However, the instability with dispersion growth rate $k(c_i)_{disp}$ results from overreflection which has a time

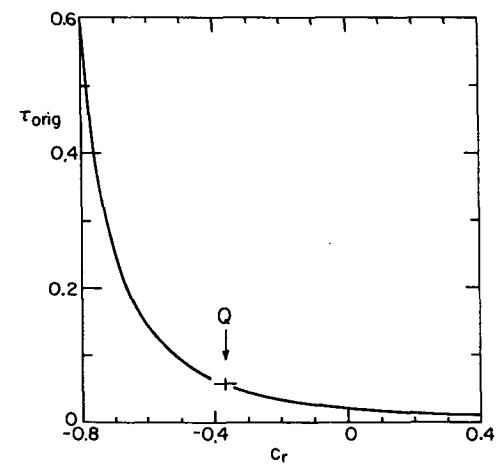

FIG. 9. Travel time τ_{orig} for a wave to travel from $z = 0$ to $z = d$ versus c_r. The c_r at which quantization occurs has been labeled with a Q. (Parameters are as in Fig. 8c.)

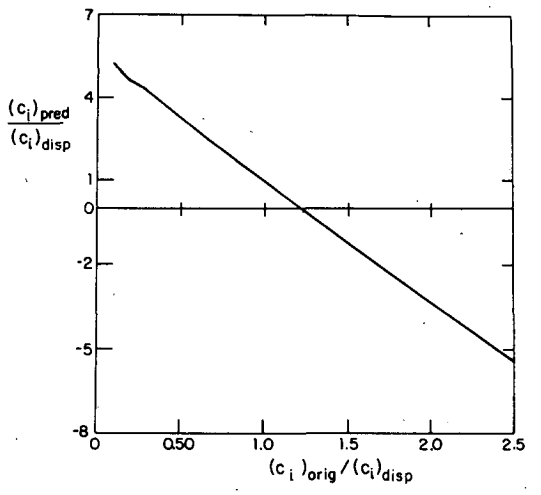

FIG. 10. $(c_i)_{pred,rR}$ [$=\ln(r_{bot}R_{sweep})/(2k\tau_{orig})$ from (38)] versus $(c_i)_{orig}$ for the case Ri = 0.24, $\mu^2 = 250$, $k = 1.2$, $L = 0.05$ and no ground. The values of c_i have been scaled by the factor $(c_i)_{disp} = 0.009537$. [Now, $(c_i)_{eig} = 0.00958$.]

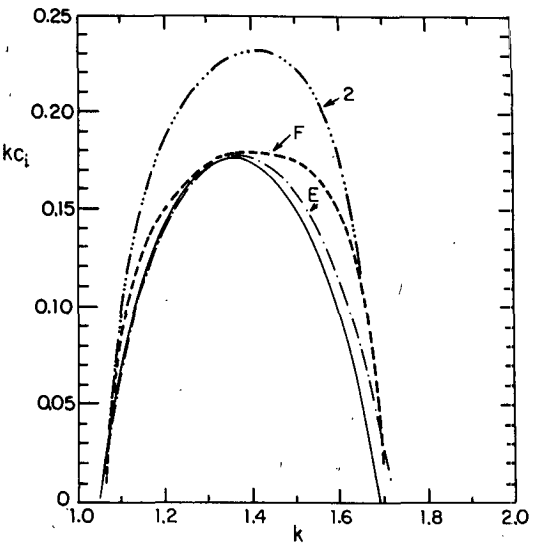

FIG. 11. This shows the same case as Fig. 4 (no ground, Ri = 0.15), with the solid line showing $k(c_i)_{disp}$ as before. Also, the curve labeled with a 2 (dashed line with 3 dots) shows the refined values of $k(c_i)_{pred}$ obtained from our first application of (A3); the dashed curve labeled with an F shows the final result obtained after the iteration defined by (A3) has converged; and the curve labeled with an E (dashed line with single dot) shows $k(c_i)_{eig}$, the growth rate obtained by solving the eigenvalue problem of finding $(c_r)_{eig}$ and $(c_i)_{eig}$ making $R_{match} = R_{sweep}$.

of order $[k(c_i)_{disp}]^{-1} \equiv \tau_d$ to develop. When $\tau_d < \tau_0$ [which is the case when $(c_i)_{orig} < (c_i)_{disp}$], the actual time available for development of overreflection is less than the time in which the reflection coefficients calculated using $(c_i)_{orig}$ are being allowed to develop. Hence, when $\tau_d < \tau_0$, the reflection coefficients calculated using $(c_i)_{orig}$ are larger than those which can be attained in time τ_d, and our estimate of the growth rate turns out to be larger than the dispersion growth rate. By similar reasoning, if the differential equation (1) is integrated with a value of $(c_i)_{orig}$ with $(c_i)_{orig} > (c_i)_{disp}$, we expect the growth rate estimated from overreflection to be less than it should be.

McIntyre and Weissman (1978) have derived expressions for the rate at which overreflection develops in a Helmholtz velocity profile. Although these expressions can be used to predict growth rates accurately for the Helmholtz velocity profile (Rosenthal, 1981), they are not applicable for the broken-line profile considered now. Instead, by considering the dependence of the predicted growth rate $k(c_i)_{pred}$ on $k(c_i)_{orig}$ (as shown in Fig. 10), we can develop an algorithm to predict the growth rate which is self-consistent with the growth resulting from the overreflection that develops in the time $(kc_i)^{-1}$. This algorithm is described in the Appendix.

Results for our second estimate of $(c_i)_{pred,rR}$ from overreflection (obtained from one iteration with (A3) and called c_3 in the Appendix) are shown in Fig. 11 by the curve labeled with a "2" for the case shown in Fig. 4 with Ri = 0.15 and no ground, and in Fig. 12, for the case shown in Fig. 5 with Ri = 0.15 and $\hat{H} = 3.24$. We also show in Figs. 11 and 12, by a curve labeled with an "F," the values obtained by iteratively using (A3) until $|(c_{n+3} - p_{n+1})/p_{n+1}|$ < 0.005. (This convergence criterion was usually satisfied after five iterations.) The improvement in the ability of these estimates of the growth rate from overreflection in Figs. 11 and 12 to approximate the growth rate obtained from the dispersion relation (shown by a solid line in Figs. 4, 5, 11 and 12) over

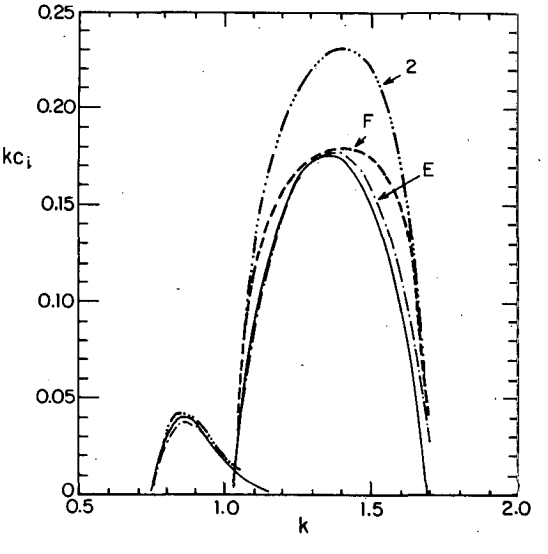

FIG. 12. This shows the same case as Fig. 5 ($\hat{H} = 3.24$, Ri = 0.15), and uses the same notation as in Fig. 11.

the ability of our initial estimate $k(c_i)_{\text{pred},rR}$ shown in Figs. 4 and 5 to estimate the growth rate is remarkable.

We also show in Figs. 11 and 12, by the line labeled with an "E," the growth rates obtained by using a two dimensional secant method (Lindzen and Rosenthal, 1976) to find the values of c_r and c_i that make the complex numbers R_{match} [as in (30)], if no ground is present, or as in (34), if a lower boundary is present) and R_{sweep} [as in (25)] equal. These figures show that this growth rate, which is the eigenvalue growth rate for the actual velocity profiles such as shown in Fig. 1 or as given by (12), is close to the dispersion growth rate, which is equivalent to the eigenvalue growth rate for a velocity profile of the form given by (12) in the limit $\mu \to \infty$ and $L \to 0$. The small difference between these growth rates shows the unimportance of variations of the quantities μ and L [which determine the curvature in the regions of high vorticity gradient in the basic velocity profile $u(z)$] from very large μ and $L \to 0$ to the actual values used. Thus, considering overreflection in the region where Kelvin–Helmholtz instabilities propagate vertically can provide quantitatively, as well as qualitatively, useful estimates of the growth rate for a velocity profile with arbitrary curvature in the regions of high vorticity gradient in the basic velocity profile.

4. Concluding remarks

We have shown that Kelvin–Helmholtz instabilities, as well as gravity wave instabilities, result from wave overreflection, with their energy extracted from the mean flow. The Kelvin–Helmholtz waves are associated with vertical propagation in regions of large vorticity gradient. Such waves have reflection coefficients R_{sweep} of the same order as those of gravity waves. However, there is a basic difference in the vertical extent of the waveguide for the two instabilities. Kelvin–Helmholtz instabilities propagate vertically in regions of large vorticity gradient bounded by internal turning points within the shear layer, whereas gravity waves propagate vertically due to stratification in the fluid in regions which may extend to the ground. The shorter travel time between successive overreflections for Kelvin–Helmholtz instabilities than for gravity waves results in Kelvin–Helmholtz instabilities generally having larger growth rates than gravity waves in profiles where the two coexist. Also, the short travel time between successive overreflections implies a short time available for overreflection to develop, which provides an explanation for why overreflection can lead to overestimates of the growth rate. We showed that the time available for the development of overreflection is of order $1/(kc_i)$.

Acknowledgments. The authors wish to acknowledge the support of the National Science Foundation under Grant ATM-78-23330 at Harvard and Grant ATM-802-3523 at M.I.T., and the National Aeronautics and Space Administration under Grant NGL-22-007-228.

APPENDIX

Prediction of the Growth Rate kc_i

We now describe an algorithm which enables growth rate estimates $k(c_i)_{\text{pred},rR}$ [found from overreflection allowed to develop for a time $1/(kc_i)_{\text{orig}}$] to be corrected to be consistent with the actual time available for the overreflection to develop. This algorithm is suggested by Fig. 10, which shows the values of $(c_i)_{\text{pred},rR}$ as a function of $(c_i)_{\text{orig}}$, for the sample case of no lower boundary with Ri = 0.24 just above $z = d$, $\mu^2 = 250$, $L = 0.05$, $z_T = 1.1$ and $k = 1.2$. When preparing Fig. 10, at each new $(c_i)_{\text{orig}}$, we adjust the number of points M in our integration to satisfy the criterion of Eq. (14), find the value of c_r that satisfies the quantization condition that the phase of R_{sweep} in (25) equals the phase of R_{match} in (30), and then predict c_i using

$$(c_i)_{\text{pred},rR} = \frac{\ln(r_{\text{bot}} R_{\text{sweep}})}{2k\tau_{\text{orig}}}$$

from (38). Fig. 10 shows that values of $(c_i)_{\text{pred}}$ from overreflection vary approximately linearly with $(c_i)_{\text{orig}}$; moreover, when $(c_i)_{\text{orig}} = (c_i)_{\text{disp}}$, we find $(c_i)_{\text{pred}} \approx (c_i)_{\text{disp}}$.

This coincidence of $(c_i)_{\text{pred},rR}$ from (38) with $(c_i)_{\text{orig}}$ in the special case that $(c_i)_{\text{orig}} = (c_i)_{\text{disp}}$ suggests an algorithm for estimating $(c_i)_{\text{disp}}$. Physically, the essence of this algorithm is to predict that kc_i which is consistent with both the overreflection in the lower waveguide and the time $1/(kc_i)$ available for the development of the overreflection. Mathematically, this algorithm involves first using two different values of $(c_i)_{\text{orig}}$, henceforth called c_n and c_{n+1}, to predict two values of $(c_i)_{\text{pred},rR}$ using (38) from overreflection, henceforth called p_n and p_{n+1}. We next estimate a value of c_{n+2} which would enable the overreflection that can develop in time $1/(kc_{n+2})$ to consistently predict the growth rate by requiring

$$c_{n+2} = p_{n+2}. \tag{A1}$$

A value of c_{n+2} that satisfies (A1) can be found graphically by linear interpolation on a graph such as Fig. 10, or by solving

$$\frac{c_{n+2} - c_n}{p_{n+2} - p_n} = \frac{c_{n+1} - c_n}{p_{n+1} - p_n}. \tag{A2}$$

After using (A1), (A2) yields

$$c_{n+2} = c_n + (c_{n+2} - p_n)\frac{(c_{n+1} - c_n)}{(p_{n+1} - p_n)},$$

which in turn yields

$$c_{n+2} = \frac{c_n p_{n+1} - p_n c_{n+1}}{p_{n+1} - p_n - c_{n+1} + c_n},$$
$$n = 1, 2, 3, \ldots. \tag{A3}$$

Then, we could use this value of c_{n+2} to predict the new value $(c_i)_{\text{pred},rR}$, p_{n+2}, from overreflection and invoke (A3) again.

In practice, we start this iterative procedure with $c_1 = (c_i)_{\text{orig}}$ and arbitrarily take $c_2 = 0.32$, for example, as our second value of $(c_i)_{\text{orig}}$ to integrate the differential equation (1). After five iterations, we generally find the values predicted by (A3) satisfy the convergence criterion $|(c_{n+3} - p_{n+1})/p_{n+1}| < 0.005$. The resulting kc_i is the predicted growth rate which is self-consistent with the overreflection that can develop in time $(kc_i)^{-1}$.

REFERENCES

Lindzen, R. S., and H. L. Kuo, 1969: A reliable method for the numerical integration of a large class of ordinary and partial differential equations. *Mon. Wea. Rev.*, **97,** 732–734.

——, and A. J. Rosenthal, 1976: On the instability of Helmholtz velocity profiles in stably stratified fluids when a lower boundary is present. *J. Geophys. Res.*, **81,** 1561–1571.

——, B. Farrell and K. K. Tung, 1980: The concept of wave overreflection and its application to baroclinic instability. *J. Atmos. Sci.*, **37,** 44–63.

McIntyre, M. E., and M. A. Weissman, 1978: On radiating instabilities and resonant overreflection. *J. Atmos. Sci.*, **35,** 1190–1196.

Rosenthal, A. J., 1981: Gravity-wave and Kelvin–Helmholtz instabilities in stably stratified shear flows. Ph.D. thesis, Harvard University, 331 pp.